Wave Propagation over a Bar and Wave Induced Bed Pressure Gradients.

Dr. ing. Øivind A. Arntsen[1]

Abstract

Wave induced pore pressure and instantaneous liquefaction are known to occur and cause loss of bearing capacity of sand. Wave bottom pressure $\bar{p}$ forms the boundary condition for the wave induced pore pressure. It is believed that not only variation of the pressure itself, but also the variations of its first and second order spatial derivative play an important role in the formation of liquefaction. An experimental and a preliminary numerical study on unidirectional water wave propagation over a bar are presented. Emphasis is placed upon investigation on the wave induced pressure gradient at the seabed. Single sinusoidal, two-component sinusoidal and five-component sinusoidal waves are investigated in a wave flume of constant water density ρ. Only the results for single sinusoidal waves are reported herein. The variation of the dimensionless pressure gradient $C_p = (\partial \bar{p} / \partial x) / (\rho g)$ was within ± 0.4 for all experiments with a tendency of larger values for downslope gradients (negative values) than for upslope. (g is the acceleration gravity). The numerical results, based on the two-dimensional Green-Naghdi theory for fluid sheets - level II, compare well for sea bed pressures and gradients, but the sea surface does not fit the observations so well.

The Numerical Model

Introduction

A new generation water wave model concept has developed during the last two decades. Its fundamental principle is known as the Green-Naghdi theory of fluid sheets,

[1] Associate professor, Department of Structural Engineering, NTNU, N-7034 Trondheim, Norway.
E-mail: oivind.arntsen@bygg.ntnu.no

hereafter referred to simply as GN theory (Green, Laws and Naghdi, 1974). The foundation for its application in water waves is discussed in the original work of Green and Naghdi (1986, 1987).

Webster and Kim (1990) use this theory to investigate the dispersion of large amplitude gravity waves in deep water. A level III GN-theory (a nonlinear 2D fluid sheet model) is used to simulate a train of steep regular waves and a random wave record corresponding to steep seas measured during hurricane Camille. An analysis of the simulated random wave record shows that linear dispersion, Airy theory with Wheeler stretching, often assumed for referring a random wave train from one point in space to another, does not result in conservative estimates of two important quantities used in design: the crest elevation and particle velocity under the crest. In regular waves the model reproduce (and confirmed by laboratory experiments) the tendency that the leading edge of a packet of relatively steep waves always appears to break before very many waves are created.

Demirbilek and Webster (1992a,1992b) derived a version of the GN-theory applicable for shallow water to moderate water depths and where the water depth may vary rapidly. The model named GNWAVE3 is as a nonlinear 2D numerical wave flume that simulates the wave transformation in shallow water in a finite difference scheme. Areas of applications may be wave transformation over submerged obstacles, reflections of waves, time history of bottom-mounted pressure gage measurements for estimation of surface wave conditions in coastal design projects. The theory is particularly suited for the collision of waves with natural and man-made structures, and their impact on preventive and hydraulic structures. The model is intended to be implemented in the Coastal Modeling System (CMS) provided by the Waterways Experiment Station, U.S. Army Corps of Engineers, Vicksburg , USA.

The purpose of using GNWAVE3 in this project is to study the feasibility of its application on the computation of wave motion over a bar. Later, it would be of interest to compare the performance of this model to results obtained with numerical wave flumes based on more conventional wave models (e.g. the Boussinesq formulation) and with more data from field and/or laboratory experiments.

Overview of theory

This overview follows the description of the model development given in Demirbilek and Webster (1992a). The GN approach to water wave theory is fundamentally different from the perturbation methods used in classical wave theory. In contrast to the Stokes and Boussinesq theories, the equations of motion in the GN theory are derived by enforcing exact kinematic and dynamic boundary conditions on the free surface and on the bottom, and by enforcing conservation of mass, but approximating the conservation of momentum. In short, the treatment of the field equation and nonlinear boundary conditions by perturbation methods and GN theory are the antithesis of one another. The essential clue of GN wave theory is that the vertical dependence of the kinematics of the fluid flow is restricted and prescribed a-priori. That is, a set of shape-functions (like the e^{kz} in deep water Airy theory) that serve as a basis for the vertical dependence is introduced. In this way the method achieves a simplification by reducing the computational domain from three dimensions to two (or from two dimensions to one in the case of 2D flows). The theory also yields governing equations for the flow, which are solved numerically in a more efficient manner than those from a conventional finite-difference, finite-element or similar schemes.

In the following, the theoretical development behind GNWAVE3 is outlined. Although GNWAVE3 is a model for 2D inviscid flow, the development of GN theory in general is not at all limited to such fluids. The governing equations are the GN level II shallow water equations originally constructed by Shields (1986) and reported by Shields and Webster (1988). The coordinate system Oxyz, with the Oz axis oriented vertically up and the Oxy plane horizontal and corresponding to the undisturbed free surface. We assume that the fluid velocity $v(x,y,z;t) = (u,\ 0,\ w)$ can be approximated as

$$v(x,z;t) = \sum_{n=0}^{2} W_n(x;t)\,\psi_n(z) \tag{1}$$

where

$$W_n = (u_n, 0, w_n)\ ; \quad n = 0,1,2 \tag{2}$$

are vector coefficients associated with the shape-functions $\psi_n(z)$. The vector coefficients are unknown spacial- and time-dependent functions to be determined as a part of the solution. In the general GN-theory the number of shape-functions is not fixed to three. The theory put restrictions on the choice of shape-functions to those that possess the following property:

$$\frac{d\psi_m}{dz} = \sum_{r=0}^{n} a_r^m\ \psi_r\ , \qquad (n \le m) \tag{3}$$

a_r^m are some constants. There are many function sets that satisfy (3). For instance, Webster and Kim (1990) use $\psi_n(z) = z^n\ e^{az}\ ,\ n = 0,1,2$ as their set of shape-functions for deep-water waves. In GNWAVE3 polynomial functions $\psi_n(z) = z^n$ form the shape-function set. The linear function $\psi_1 = z$ was selected since it coincides with the z dependence found in linear shallow water wave theory.

The kinematic assumption (1) is inserted into the equations for conservation of mass, conservation of momentum (Euler equations), and the kinematic boundary conditions on the free surface $z = \beta(x;t)$ and at the bottom $z = \alpha(x,t)$. These equations are all satisfied identically by this method. When (1) is substituted into the momentum equation and the resulting equation is required to be satisfied everywhere in the fluid domain, many more equations than the required number would be obtained. To overcome this difficulty, the shape-functions ψ_m are used as weighting functions to develop the required number of equations to be solved. Euler's equations are multiplied by each $\psi_n(z)$ and integrated from the sea bottom to the free surface. The weighted momentum equations express the conservation of momentum in some integral sense and consequently the conservation of momentum is satisfied only approximately. The determination of the evolution equations in terms of derivatives of the primary variables requires a prodigious amount of algebraic manipulation. For theory of level I or of level II it is not too difficult to obtain this by hand, however, for higher level of the theory mathematical symbolic processors should be used.

In GNWAVE3 the velocity profile is modeled as

$$u(x,z;t) = u_0(x;t) + u_1(x;t)z + u_2(x;t)z^2 \tag{4}$$

$$w(x,z;t) = w_0(x;t) + w_1(x;t)z + w_2(x;t)z^2 \tag{5}$$

Fulfillment of the continuity equation implies that $u_2(x;t) \equiv 0$, and consequently the horizontal velocity profile is restricted to linear variation with depth.

It is now possible to eliminate the vertical vector coefficients as well as the integrated pressure coefficients. The final sets of governing equations involving the three unknown functions $\beta(x;t)$, $u_o(x;t)$, $u_1(x;t)$ (free surface elevation and the two remaining coefficients of the horizontal velocity respectively) are rather difficult to derive without the help of mathematical symbolic software.

Although the equations may seem large and complicated they may be integrated with little difficulty. Together they form a system of three coupled, partial differential equations that are of first order in time and of third order in space and the highest order of mixed derivatives are of first order in time and second order in space. Thus the system of equations can be summarized as

$$\boldsymbol{A}\dot{\xi} + \boldsymbol{B}\frac{\partial\dot{\xi}}{\partial x} + \boldsymbol{C}\frac{\partial^2\dot{\xi}}{\partial x^2} = \boldsymbol{g}\,; \qquad \xi \equiv (\beta, u_0, u_1)^T. \tag{6}$$

The matrices $\boldsymbol{A}$, $\boldsymbol{B}$, $\boldsymbol{C}$ and the vector $\boldsymbol{g}$ are functions of x and β, u_0, u_1 and their derivatives. With prescribed boundary conditions at both ends of the domain the equations can be solved through a numerical technique. The domain of x over which a solution to the equations is desired is assumed to be a finite difference scheme of uniformly spaced grids in the x-direction spaced a distance Δx apart. Time is assumed to be discretised with intervals Δt. The spatial distribution of $\dot{\xi}$ is first found by a central difference technique combined with a forward backward substitution. The updated values for ξ is obtained through a two step forward explicit scheme.

The Pressure Relation

Taking the vector dot product between the vectored equations of motion and the vertical unity vector e_3 and integrating from the sea bed to the free surface, we obtain an explicit expression for the bottom pressure (e_1 is the x-direction unity vector).

$$\int_\alpha^\beta \left(\frac{\partial(\rho v)}{\partial t} + u\frac{\partial \rho v}{\partial x} + w\frac{\partial \rho v}{\partial z} \right) \cdot e_3 dz = \int_\alpha^\beta \left(-\frac{\partial p}{\partial x} e_1 - \frac{\partial p}{\partial z} e_3 - \rho g e_3 \right) \cdot e_3 dz$$

$$\Downarrow \tag{7}$$

$$\int_\alpha^\beta \left(\frac{\partial(\rho v)}{\partial t} + u\frac{\partial \rho v}{\partial x} + w\frac{\partial \rho v}{\partial z} \cdot e_3 \right) dz = \int_\alpha^\beta \left(-\frac{\partial p}{\partial z} - \rho g \right) dz = -\left(p_\beta - p_\alpha\right) + \rho g(\alpha - \beta)$$

Assuming the surface pressure p_β equal to zero and denoting the bottom pressure $p_\alpha \equiv \overline{p}$ this results in:

$$\overline{p} = -\rho g(\alpha - \beta) + \int_\alpha^\beta \left(\frac{\partial(\rho v)}{\partial t} + u\frac{\partial \rho v}{\partial x} + w\frac{\partial \rho v}{\partial z} \cdot e_3 \right) dz \tag{8}$$

Within the limits of level II theory and uneven bottom this expression can be rewritten in terms of the variables u_0 and u_1 and their derivatives with respect to time and horizontal variation and β in addition to the known bottom variation $\alpha(x)$. The resulting equation is:

$$\overline{p} = \overline{p}_r + \overline{p}_{u_0 t}\frac{\partial u_0}{\partial t} + \overline{p}_{u_0 tx}\frac{\partial^2 u_0}{\partial x \partial t} + \overline{p}_{u_1 t}\frac{\partial u_1}{\partial t} + \overline{p}_{u_1 tx}\frac{\partial u_1}{\partial x \partial t} \tag{9}$$

where

$$\begin{aligned}
\overline{p}_r = -\ \{ & \rho g(\alpha-\beta) - \rho(\alpha-\beta)^2\left(\frac{\partial u_0}{\partial x}\right)^2 / 2 + \rho\left(\frac{\partial \alpha}{\partial x}\right)^2 (\alpha-\beta)u_1\left(2u_0 + (\alpha+\beta)u_1\right)/2 \\
& + \rho\frac{\partial^2 \alpha}{\partial x^2}(\alpha-\beta)(u_0+\alpha u_1)(2u_0+(a_0+\beta)u_1)/2 \ - \ \rho\frac{\partial \alpha}{\partial x}(-\alpha+\beta)\frac{\partial u_0}{\partial x}(u_0+\beta u_1) \\
& + \rho(\alpha-\beta)^2\frac{\partial^2 u_0}{\partial x^2}\left(3u_0 + (\alpha+2\beta)u_1\right)/6 \ - \ \rho(\alpha-\beta)^2(\alpha+\beta)\frac{\partial u_0}{\partial x}\frac{\partial u_1}{\partial x}/2 \\
& + \rho\frac{\partial \alpha}{\partial x}(\alpha-\beta)\left((3\alpha-\beta)u_0 + \alpha(\alpha+\beta)u_1\right)\frac{\partial u_1}{\partial x}/2 \ - \ \rho(\alpha-\beta)^2(\alpha+\beta)^2\left(\frac{\partial u_1}{\partial x}\right)^2/8 \\
& + \rho(\alpha-\beta)^2\left(4(2\alpha+\beta)u_0 + 3(\alpha+\beta)^2 u_1\right)\frac{\partial^2 u_1}{\partial x^2}/24\}
\end{aligned}$$

$\overline{p}_{u_0 t} = -\frac{\partial \alpha}{\partial x}(\alpha-\beta)\rho$, $\overline{p}_{u_0 tx} = -(\alpha-\beta)^2\rho/2$, $\overline{p}_{u_1 t} = -\alpha\frac{\partial \alpha}{\partial x}(\alpha-\beta)\rho$ and $\overline{p}_{u_1 tx} = -(\alpha-\beta)^2(2\alpha+\beta)\rho/6$.

Initial Conditions

For this shallow water study it is assumed that the time history of the waves is known at $x = 0$. The waves are input not only as local wave height history $\beta(0,t)$, but also as a history of the corresponding values of the other variables in this Level II theory ($u_0(0,t)$ and $u_1(0,t)$). These variables are obtained from the solution of steady waves on a flow (linearized for small wave amplitude and flow speed = - celerity of the waves). These linear solutions for waves propagating with a celerity c are:

$$\beta(0,t) = \beta_0 \cos(kx - \omega t) = \beta_0 \cos(k(x - ct)) \tag{10}$$

$$u_0(0,t) = \beta_0 \frac{12g\left(20 + 7(kd_S)^2\right)}{c\left(240 + 104(kd_S)^2 + 3(kd_S)^4\right)} \cos(\omega t) \tag{11}$$

$$u_1(0,t) = \beta_0 \frac{120g(kd_S)^2}{cd_S\left(240 + 104(kd_S)^2 + 3(kd_S)\right)} \cos(\omega t) \tag{12}$$

$$c = \sqrt{\frac{24gd_S\left((kd_S)^2 + 10\right)}{240 + 104(kd_S)^2 + 3(kd_S)^4}} \tag{13}$$

where d_S is the still water depth at the wave generator and g is the acceleration of gravity. Thus, $u(0,z,t) = u_0(0,t) + u_1(0,t)\,z$ is the horizontal particle velocity at the wave paddle. Here z is measured positive upwards from the seabed. Figure 1 compares the distribution to that obtained from Airy wave theory, in the case of a $T = 2.3$ s wave period and a H=0.2 m high wave in water depth of 0.6 m and of a 9.65 s wave of 3.0 m height in 35 m waterdepth.

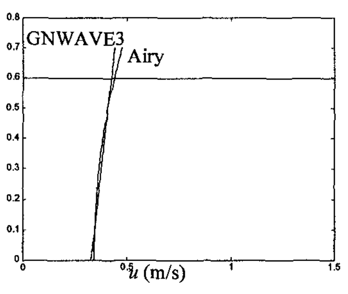

a) $H = 0.2$ m, $T = 2.3$ s, $d_S = 0.6$ m

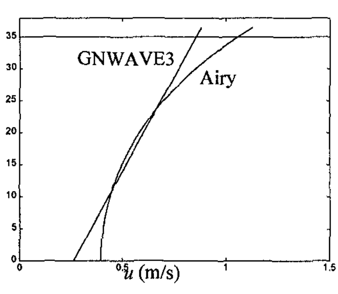

b) $H = 3.0$ m, $T = 9.65$ s, $d_S = 35$ m.

Figure 1. Wavemaker boundary conditions (horizontal particle velocity) in GNWAVE3 compared to Airy linear wave theory.

The boundary condition at the other end of the wave flume is modeled either as fully reflective or fully open.

GNWAVE3 Performance Example

A simple test run of GNWAVE3 shows its capability of time-simulation of waves. This test run is performed with wave-data from one of the experimental runs, but with constant water depth equal to 0.70 m. Other inputs to the model is the same as for the reference experiment *bp136150* described later. A time-series recording at x=5 meters is shown in Figure 2 and a snapshot of the surface elevation after 39.95 seconds is shown in Figure 3. The time function in Figure 2 has been analyzed with respect to zero-upcrossings and also a peak-to-peak analysis to establish two sequences of wave periods. Similarly the function in Figure 3 has been analyzed with respect to zero-upcrossings, and the sequence of identified wave-lengths was found. The results are seen in Figure 4 together with the average values. In Table 1 the derived wave parameters are compared to values obtained by Airy wave theory and by an analytical nonlinear model known as the Fourier-series model, both available in (ACES, 1992). The Fourier-series model requires knowledge of the vertically integrated flow in the flume. It was set equal to zero in this example.

GNWAVE3, which is a numerical model based on the first principles of conservation of momentum and continuity of mass demonstrates stability and accuracy that of sufficient quality for this example test. E.g. the deviations between GNWAVE3 results and Airy theory are less 0.5 % both in wavelength and celerity.

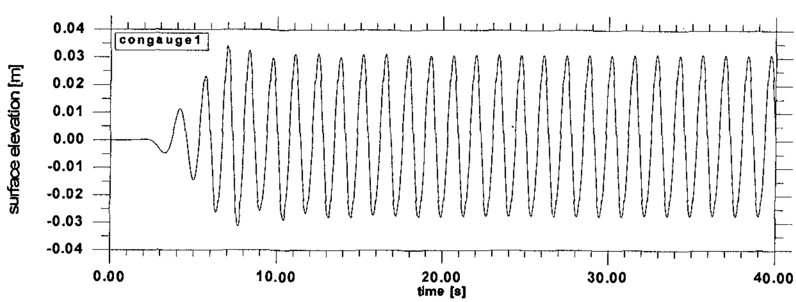

Figure 2. Time-series of the surface elevation at x = 5 meters.

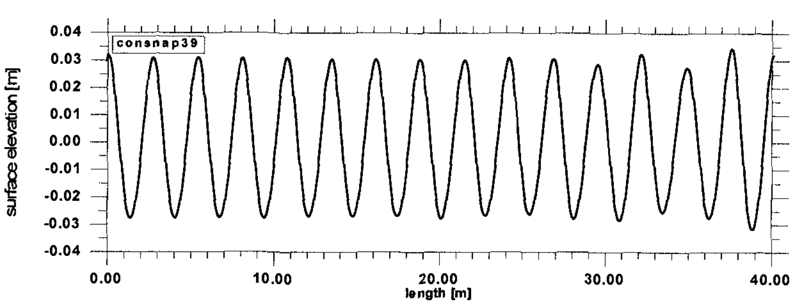

Figure 3. Snapshot of the surface at time 39.95 sec.

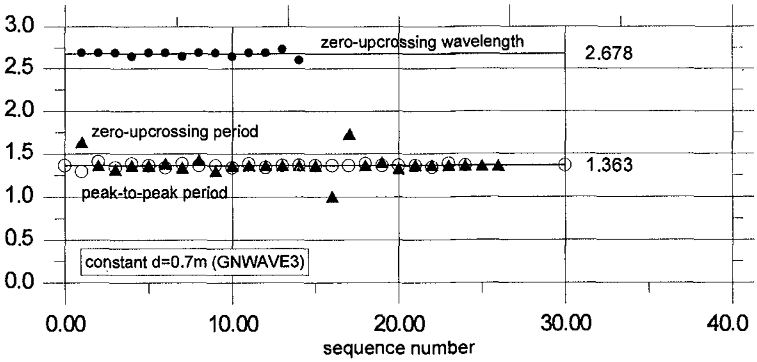

Figure 4. Sequences of wavelengths and wave periods

Table 1. Wave parameters computed from three different wave models

Parameter (input) Froude scaling	GNWAVE3 protype values (M=1:50)	AIRY THEORY protype values (M=1:50)	FOURIER-SERIES protype values (M=1:50)
H (3.00 m)	2.90 m (num. res.)	3.00 m (input)	3.00 m (input)
T (9.645 s)	9.638 s (num. res.)	9.645 s (input)	9.645 s (input)
d (35.0 m)	35.0 m (input)	35.0 m (input)	35.0 m (input)
λ	133.9 m (num. res.)	134.5 m (num. res.)	135.0 m (num. res.)
c	13.89 m/s (num.res.)	13.95 m/s (num. res.)	13.98 m/s (num. res.)

Laboratory Experiments

Setup

The experimental setup is shown in Figure 5. The experiments were carried out in a wave flume with a trapezoidal bar. The flume is 40 m long, 5m wide. Around the bar the water depth was 0.70 m, on the bar plateau the depth was 0.25 m. Free surface waves were measured by parallel-wire resistance gauges at three stations. Two pressure sensors of type Kistler 4043 were installed in the sea bed near the top break of the slope at a location were waves were expected to break. The numerical model was gauged at the same five locations, see Table 2 and Figure 5. Gauge 1 measures surface elevation at the beginning of the slope, Gauge 2 measures the surface elevation near the top break of the slope, Gauge 3 measures the surface elevation on the bar plateau. Gauge 4 and Gauge 5 measures bottom pressures at Gauge 2, from which the bottom pressure gradient can be estimated by computing the differences. All the gauges were leveled to zero before each run, thus only the dynamical part of the processes were recorded. The accuracy of the gauges is indicated in Table 2. However some zero-drift was detected during the analysis of data, thus the mean levels of the processes have been somewhat adjusted before the final presentation.

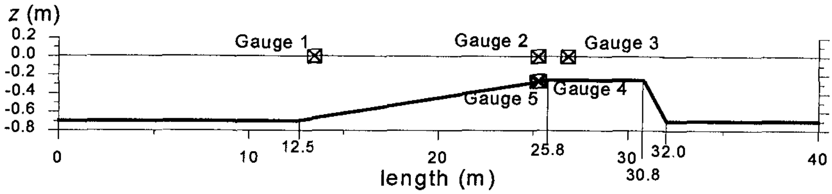

Figure 5. Experimental set up. Measures in meters.

Table 2. Gauge locations and accuracy

Gauge	process	x (m)	z (m)	accuracy
1	water level, η_1	13.42 (x_1)	0.000	$\pm 2mm$
2	water level, η_2	25.25 (x_2)	0.000	$\pm 2mm$
3	water level, η_3	26.82 (x_3)	0.000	$\pm 2mm$
4	pressure , p_4	25.30 (x_4)	-0.265	$\pm 50Pa$
5	pressure, p_5	25.20 (x_5)	-0.268	$\pm 50Pa$

Results

The experiments included one-component, two-component and five-component sinusoidal waves. The results shown below are for one-component waves only. Preliminary inspection of the other runs reveals similar pressure gradients . Results for both breaking and nonbreaking waves are included. Table 3 summarizes the results in which;

- H_1 is an estimate for the wave height at Gauge 1; $= (\eta_{1,\max} - \eta_{1,\min})$.
- T is an estimate for the wave period = average time between peeks over about a 20 s interval.
- H_2 is an estimate for the wave height at Gauge 2; $= (\eta_{2,\max} - \eta_{2,\min})$.
- H_0 is the deep water wave height given by the Airy theory shoaling coefficient (computed from H_1, T and d_1; d_1 - the still water depth at Gauge 1).
- λ_0 is the deep water wave length; $= gT^2 / 2\pi$.
- λ_S is the wave length in the constant depth part of the flume in front of the slope determined by the Airy wave theory: $\lambda_S = 2\pi/k_S$ where k_S is given by: $\omega^2 = gk_S \tanh k_S d_S$ and $\omega = 2\pi / T$; d_S - the water depth at start of the slope).
- C_p is the dimensionless dynamic pressure gradient defined as:

$$C_p = \frac{1}{\rho g}\frac{\partial \overline{p}}{\partial x} \approx \frac{1}{\rho g}\frac{p_4 - p_5}{x_4 - x_5} \quad . \tag{14}$$

  Column of positive index refers to positive values, column of negative index refers to negative values.
- H_2/d_2 is a breaking wave index (rule of thumb: waves break for approx. 0.78). (d_2 = depth at Gauge 2).

- ξ is a local Irribarren number defined as $\xi = \ \mathrm{tg}\theta / \sqrt{H_2 / \lambda_0}$.
- Ir is the Irribarren number based on deep water wave height, i.e. $Ir = \ \mathrm{tg}\theta / \sqrt{H_0 / \lambda_0}$

The three latter parameters are used as dimensionless variables for graphical presentation. They appear to be powerful parameters to determine for which wave conditions large pressure gradients are favorable. Figure 6 shows the variability of C_p with respect to these dimension-less numbers. It is seen that the values of C_p are all within ±0.4 and that the largest values occur for the steepest waves just about breaking. The Irribarren number is often used for breaker type classification (Battjes, 1974), as listed below in Table 3. According to this table all runs should have resulted in spilling breakers. That was not the case. In Table 4 is listed the observed type of breakers. When these observations are held together with the results in Table 3, we see that the plunging breakers are associated with the largest values of C_p. $|C_p|$<0.4 is believed not sufficient to cause liquefaction in a saturated seabed. If the seabed contains a fraction of gases these levels may be sufficient. (Moshagen, 1997).

Table 3 Summary of the wave conditions and the main derivations

reference	H_1 [cm]	T [s]	H_2 [cm]	H_0[cm]	λ_0[cm]	λ_S [cm]	C_{p+} [-]	C_{p-} [-]	H_2/d_2 [-]	ξ [-]	Ir [-]
bp100100	13.8	1.07	13.1	14.2	179	176	0.22	0.23	0.49	0.123	0.118
bp100120	16.6	1.07	17.8	17.1	179	176	0.25	0.27	0.67	0.106	0.108
bp100121	17.1	1.07	18.1	17.6	179	176	0.27	0.26	0.68	0.105	0.106
bp100130	19.2	1.07	19.5	19.8	179	176	0.23	0.27	0.74	0.101	0.100
bp100140	20.0	1.07	19.8	20.6	179	176	0.24	0.29	0.75	0.100	0.098
bp100150	18.2	1.07	19.1	18.8	179	176	0.23	0.29	0.72	0.102	0.103
bp116150	22.3	1.18	16.2	23.7	217	210	0.22	0.20	0.61	0.122	0.101
bp126150	19.1	1.25	22.1	20.3	244	232	0.25	0.35	0.83	0.111	0.116
bp136150	18.1	1.36	22.0	19.5	289	268	0.24	0.36	0.83	0.121	0.128
bp145150	18.1	1.45	22.0	19.7	328	296	0.24	0.36	0.83	0.129	0.136
bp154150	15.8	1.55	22.3	17.3	375	326	0.33	0.37	0.84	0.137	0.155
bp160150	15.9	1.56	21.5	17.4	380	330	0.27	0.31	0.81	0.140	0.156
bp165150	15.2	1.65	23.0	16.6	425	358	0.23	0.37	0.87	0.143	0.169
bp200200	17.2	2.13	22.6	18.3	708	500	0.22	0.33	0.85	0.187	0.207
bp300100	6.7	3.15	8.4	6.4	1548	786	0.13	0.12	0.32	0.452	0.518

Table 4 Breaker type index

Breaker type	Irribarren number
Spilling	$0 < Ir < 0.5$
Plunging	$0.5 < Ir < 3.3$
Surging, collapsing	$3.3 < Ir$

Table 5 Observed breaker type and location of regular waves.

reference	remarks
bp100100	No breaking waves on the slope. The wave broke approx. 3.5 m past Gauge 3.
bp100120	Spilling/Plunging breaker occurred approx. 0.8 m past Gauge 2.
bp100121	Spilling/Plunging breaker occurred approx. 0.8 m past Gauge 2.
bp100130	Spilling breaker occurred approx. 0.8 m in front of Gauge 2.
bp100140	Spilling breaker occurred approx. 1.5 m in front of Gauge 2.
bp100150	Spilling breaker occurred approx. 4.0 m in front of Gauge 2.
bp116150	Spilling/Plunging breaker approx. 2.0 m in front of Gauge 2.
bp126150	Plunging breaker approx. at Gauge 2.
bp136150	Plunging breaker approx. at Gauge 2.
bp145150	Plunging breaker approx. 0.8 m behind Gauge 2.
bp154150	Plunging breaker approx. 1.2 m behind Gauge 2.
bp160150	Plunging breaker approx. midway between Gauge 2 and Gauge 3.
bp165150	Plunging breaker approx. midway between Gauge 2 and Gauge 3.
bp200200	Plunging breaker approx. at Gauge 2.
bp300100	No breaking waves.

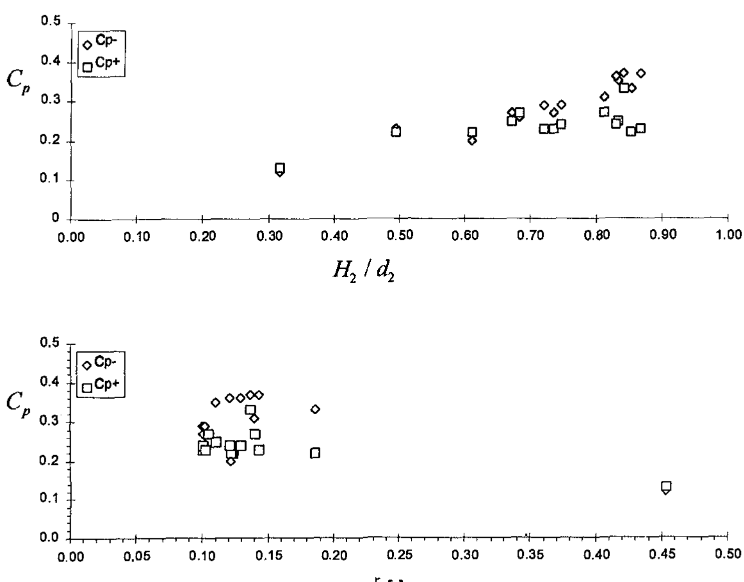

Figure 6 Variation of the dynamic pressure gradient, C_p.

Comparisons - GNWAVE3 and Experimental Results

Raw time-series plots of $\eta_1, \eta_2, \eta_3, p_4, p_5$ and C_p are available for all runs in a separate report (Arntsen, 1996). In this paper only one run will be presented. The output of the model was sampled at flume positions close to those in the physical model. However, since the model operates at discrete time and spacial steps a slight difference in locations are present. The output of the model are "snapshots" at prescribed times, and/or timeseries at prescribed positions. In this run, 5 sets of timeseries were recorded at the gauges 1-5 plus a snapshot at time 30 seconds after switching the model on. The model was set to run for 40 seconds, but collapsed due to "wave breaking" after 30.1 seconds. The spatial discretization was dx = 0.0462 m and the time discretization was dt = 0.0227 s. A snapshot of the surface elevation is shown in Figure 7, while a timeseries of the surface elevation at Gauge 2 is shown in Figure 8. Figure 9 is an intercomparison between observations and results from the numerical model for the run with reference *bp136150*. Although the fit of surface elevations are not so well in shape and phase, the model seem to predict the bed pressure fluctuations excellently. Also the amplitude of the waves before breaking is in good agreement. Breaking is identified by the "noisy" results close to the downslope break-point in Figure 7. It is believed that the model would perform better if that slope has been modeled less steep. Some of the deviations in amplitude are definitively caused by that the model has not run sufficiently long time to establish a stable solution. Cf. the initial disturbances in Figure 8. All considered, the GNWAVE3 seems to be a fairly good tool for the modeling of bed-pressure fluctuations in non-breaking shallow water waves.

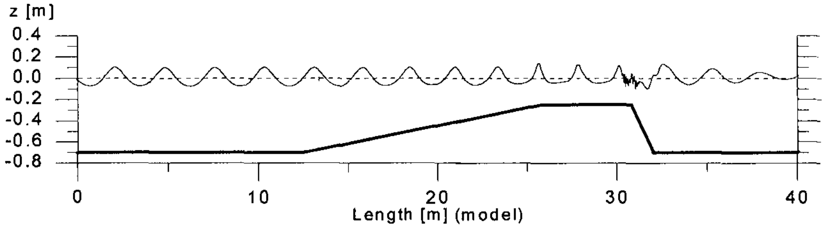

Figure 7 Snapshot of surface elevation (GNWAVE3).

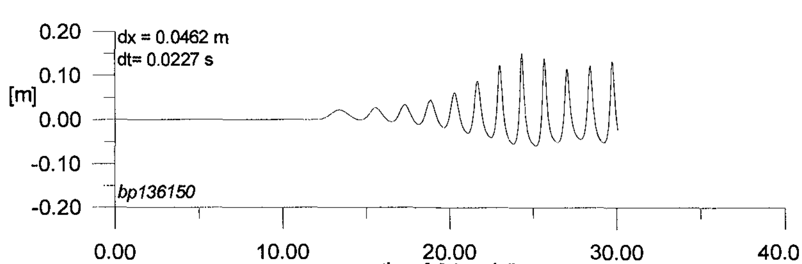

Figure 8 Timeseries of surface elevation at Gauge 2 (GNWAVE3)

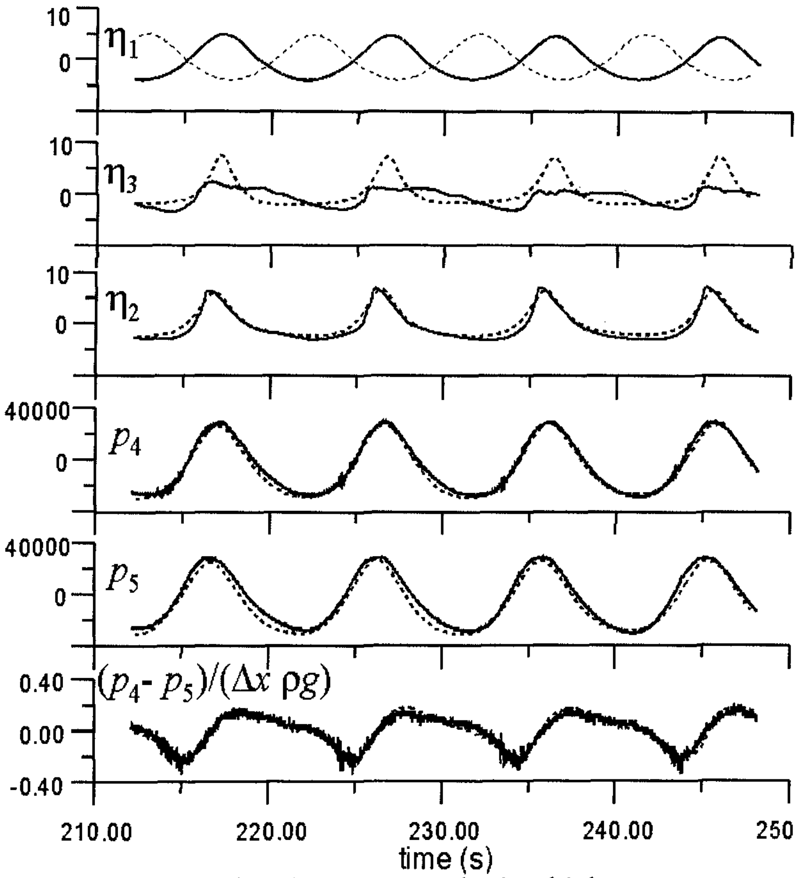

Figure 9 Intercomparisons between measured and modeled (GNWAVE3) wave dynamics over a trapezoidal bar. Prototype scale (M=1:50). H=9.1 m, T=9.6 s, d_S = 35 m. The timeseries are synchronized at Gauge 2 measurements.

Conclusions

GNWAVE3 seems to be a good tool for modeling bottom-pressure fluctuations in non-breaking shallow water waves. The observed levels of pressure gradients are believed not sufficient to cause liquefaction in a saturated seabed. However, if the seabed contains fraction of gases, these levels may be sufficient.

Acknowledgement

This study is partially supported by the Commission of the European Communities, Directorate-General XII for the Science, Research and Development Program Marine Science and Technology (MAST III) Contract No. MAS3-CT97-0097, Scour Around Coastal Structures (SCARCOST).

References.

ACES (1992). "Automated Coastal Engineering System version 1.07. Users-guide & Technical Reference." Coastal Engineering Research Center, Waterways Exp. Station, 3909 Halls Ferry Road, Vicksburg, MS 39180-6199, USA.

Arntsen, Ø.A. (1996). "Wave propagation over a bar and wave induced bed pressure. Plots of recorded time series." Department of structural engineering, NTNU, Trondheim, Norway. Misc. paper.

Battjes, J.A. (1974). "Computation of set-up longshore currents, run-up and overtopping due to wind generated waves." Communications on Hydraulics, Delft University of Technology, report 74-2.

Demirbilek, Z., and Webster, W. (1992a). "Application of the Green-Naghdi Theory of Fluid Sheets to Shallow-Water Wave Problems, Report 1, Model development." Waterways Exp. Station, Vicksburg, MS, USA. Technical Report CERC-92-11.

Demirbilek, Z., and Webster, W. (1992b). "Users Manual and Examples for GNWAVE." Waterways Exp. Station, Vicksburg, MS, USA. Technical Report CERC-92-13.

Green, A.E., Laws, N., and Naghdi, P.M. (1974). "On the Theory of Water Waves." Proc. Roy. Soc. London, A338, 43-55.

Green, A.E., and Naghdi, P.M. (1986). "A Nonlinear Theory of Water Waves for Finite and Infinite Depths." Philos. Trans. Roy. Soc. London, Ser. A320, 37-70.

Green, A.E., and Naghdi, P.M. (1987). "Further developments in a Nonlinear Theory of Water Waves for Finite and Infinite Depths." Philos. Trans. Roy. Soc. London, A324, 47-72.

Moshagen, H. (1996). Personal Communications. STATOIL, Trondheim, Norway.

Shields, J. J. (1986). "A Direct Theory for Waves Approaching a Beach." Ph.D. thesis, University of California, Berkeley, p 137.

Shields, JJ., and Webster, W. C. (1988). "On Direct Methods in Water-Wave Theory." J. Fluid Mech., Vol 197, 171-199.

Webster, W., and Kim, D.-Y. (1990). "The Dispersion of Large-Amplitude Gravity Waves in Deep Water." 10th Naval Hydrodynamic Symp., 1990, 397- 416.